

Authigenic iron oxide proxies for marine zinc over geological time and implications for eukaryotic metallome evolution

L. J. ROBBINS,¹ S. V. LALONDE,² M. A. SAITO,³ N. J. PLANAVSKY,⁴ A. M. MLOSZEWSKA,¹ E. PECOITS,¹ C. SCOTT,⁵ C. L. DUPONT,⁶ A. KAPPLER⁷ AND K. O. KONHAUSER¹

¹Department of Earth & Atmospheric Sciences, University of Alberta, Edmonton, AB, Canada

²UMR 6538 Domaines Océaniques, European Institute for Marine Studies, Technopôle Brest-Iroise, Plouzané, France

³Marine Chemistry and Geochemistry Department, Woods Hole Oceanographic Institution, Woods Hole, MA, USA

⁴Department of Earth Sciences, University of California, Riverside, CA, USA

⁵Department of Earth and Planetary Sciences, McGill University, Montreal, QC, Canada

⁶Microbial and Environmental Genomics Group, J. Craig Venter Institute, San Diego, CA, USA

⁷Geomicrobiology Group, Center for Applied Geoscience, University of Tuebingen, Tuebingen, Germany

ABSTRACT

Here, we explore enrichments in paleomarine Zn as recorded by authigenic iron oxides including Precambrian iron formations, ironstones, and Phanerozoic hydrothermal exhalites. This compilation of new and literature-based iron formation analyses track dissolved Zn abundances and constrain the magnitude of the marine reservoir over geological time. Overall, the iron formation record is characterized by a fairly static range in Zn/Fe ratios throughout the Precambrian, consistent with the shale record (Scott *et al.*, 2013, *Nature Geoscience*, **6**, 125–128). When hypothetical partitioning scenarios are applied to this record, paleomarine Zn concentrations within about an order of magnitude of modern are indicated. We couple this examination with new chemical speciation models to interpret the iron formation record. We present two scenarios: first, under all but the most sulfidic conditions and with Zn-binding organic ligand concentrations similar to modern oceans, the amount of bioavailable Zn remained relatively unchanged through time. Late proliferation of Zn in eukaryotic metallomes has previously been linked to marine Zn biolimitation, but under this scenario the expansion in eukaryotic Zn metallomes may be better linked to biologically intrinsic evolutionary factors. In this case, zinc's geochemical and biological evolution may be decoupled and viewed as a function of increasing need for genome regulation and diversification of Zn-binding transcription factors. In the second scenario, we consider Archean organic ligand complexation in such excess that it may render Zn bioavailability low. However, this is dependent on Zn–organic ligand complexes not being bioavailable, which remains unclear. In this case, although bioavailability may be low, sphalerite precipitation is prevented, thereby maintaining a constant Zn inventory throughout both ferruginous and euxinic conditions. These results provide new perspectives and constraints on potential couplings between the trajectory of biological and marine geochemical coevolution.

Received 14 December 2012; accepted 8 March 2013

Corresponding author: L. J. Robbins. Tel.: +1-780-492-6532; fax: +1-780-492-2030; e-mail: lrobbins@ualberta.ca

INTRODUCTION

Zinc is the most common inorganic cofactor in eukaryotic metalloenzymes (Berg & Shi, 1996; Maret, 2001; Dupont *et al.*, 2010), and as a consequence, it has become the

basis for a hypothesis that the biological use of Zn may have evolved in the late Precambrian when it became available in seawater (Williams & da Silva, 1996; Saito *et al.*, 2003; Dupont *et al.*, 2006, 2010). Modern marine phytoplankton differ significantly in their ability to grow at low

Zn concentrations; modern surface seawater has concentrations that range from ~0.04 to 0.5 nM (e.g. Bruland, 1989; Lohan *et al.*, 2002). Studies of marine cyanobacteria have found little to no measurable Zn requirement under the conditions tested thus far in the globally abundant *Prochlorococcus* and *Synechococcus* (Sunda & Huntsman, 1995; Saito *et al.*, 2002). In contrast, eukaryotic phytoplankton have been observed to be quite sensitive to low zinc conditions. Some, notably neritic diatoms (those that inhabit shallow marine waters from the littoral zone to the edge of the continental shelf), are more sensitive and experience growth rates that are significantly reduced at free Zn^{2+} concentrations below $10^{-11.5}$ M, while others show only minor reductions in growth rates at 10^{-13} M (Brand *et al.*, 1983). The centric diatom *Thalassiosira* sp. displays dramatically reduced growth rates in coastal species at Zn concentrations of $10^{-12.5}$ M (Tortell & Price, 1996); however, species from offshore oligotrophic environments, such as *Thalassiosira oceanica*, are more tolerant of low Zn conditions (Sunda & Huntsman, 1995). The unicellular algae, *Emiliania huxleyi* (a coccolithopharad), shows decreased levels of alkaline phosphatase activity as Zn approaches picomolar concentrations (Shaked *et al.*, 2006). Concentrations are low enough in modern environments that Zn stimulation or co-limitations of marine phytoplankton communities have been observed in some high nutrient, low chlorophyll environments (Franck *et al.*, 2003; Jakuba *et al.*, 2012), but not in other environments (Crawford *et al.*, 2003; Coale *et al.*, 2005). While physiological studies of phytoplankton Zn requirements are limited and it is apparent that no single dissolved Zn concentration can be pinpointed as universally limiting, it is also apparent that severely suppressed marine Zn concentrations would have significant consequences for the activity and abundance of modern eukaryotic phytoplankton.

Such may have been the case in deep geological time. A survey of physiological experiments found that marine prokaryotic microbes, particularly the cyanobacteria, show metal nutritional requirements consistent with hypothesized Precambrian seawater compositions (Saito *et al.*, 2003). From this, it was suggested that during much of the Precambrian, the bioavailable marine Zn reservoir, as well as those of Cu and Cd, may have been much lower than in the modern oxygenated ocean due to the formation of strong aqueous complexes between Zn and sulfide that are likely not bioavailable (Luther *et al.*, 1996; Edgcomb *et al.*, 2004). Proteomic-based phylogenetic analyses also indicate a relatively late origin for most Zn-binding domains in eukaryotic metalloenzymes, leading to the suggestion that in addition to depressed oxygen availability, marine Zn biolimitation stemming from higher Precambrian sulfide concentrations and expanded euxinia during the mid-Proterozoic (1800–800 Ma) may have impeded eukaryotic diversification (Dupont *et al.*, 2006, 2010).

Accordingly, seemingly rapid eukaryotic diversification in the Neoproterozoic (1000–542 Ma) may, in part, be tied to an enhanced bioavailable marine Zn reservoir accompanying oxygenation of the oceans. This model provides a simple link between the enigmatic and protracted diversification of eukaryotes and the shifting availability of bioessential metals in a manner akin to a ‘bio-inorganic bridge’ (Anbar & Knoll, 2002).

However, until recently this possibility has yet to be evaluated in light of sedimentary proxies for the evolution of the paleomarine Zn reservoir. A recent examination of the shale record (Scott *et al.*, 2013) indicates that Zn may have been near-modern abundances and was likely bioavailable to eukaryotes throughout the Precambrian, casting doubt on the coupled geochemical and eukaryotic evolutions with respect to Zn utilization. Here, guided by new chemical speciation models, we explore eukaryotic evolution as revealed by a ~3.8-billion-year record of marine authigenic iron oxide deposition, in the form of Precambrian iron formations, Phanerozoic ironstones and Fe-rich exhalites, herein collectively referred to as iron formations (IF). We use the rock record to shed light on the poorly understood relationships between marine trace metal availability, metalloenzyme proliferation, and biological innovation.

Zn is predominantly bound by organic ligands in modern seawater (e.g., Crawford *et al.*, 2003), but it also occurs in aqueous form, that is, Zn^{2+} , $Zn(OH)^+$, $Zn(OH)_2$, $ZnCO_3$, $ZnSO_4$, and $ZnCl_2$, suspended solids (e.g., ZnS), or adsorbed onto particle (e.g., Zirino & Yamamoto, 1972). Furthermore, Zn may be strongly complexed by aqueous sulfide (Luther *et al.*, 1996) such that in anoxic environments, where HS^- is present, inorganic bisulfide and potentially polysulfide Zn complexes may play key roles in dominating the speciation of dissolved Zn (e.g., Gardner, 1974). Luther *et al.* (1999) provide an example of when polysulfides may become dominant, which occurs when 10 μ M Zn is titrated with sulfide in excess of 5 μ M. In some conditions where a strong redoxcline exists, such as Jellyfish Lake, Palau (Landing *et al.*, 1991), total dissolved Zn concentrations may actually increase at depth due to the formation of aqueous sulfide complexes. The proportion of Zn that is bioavailable is controlled by either sulfide complexation (Luther *et al.*, 1996; Edgcomb *et al.*, 2004) or by organic ligand complexation. However, complicating the issue of bioavailability is recent evidence that suggests organic complexation of Zn may in fact increase the potential for uptake (Aristilde *et al.*, 2012).

In surface layers of the open ocean, horizontal and vertical mixing, atmospheric fallout, biological uptake, and particulate removal are the main controls on Zn abundance (Bruland, 1980). Accordingly, total dissolved Zn follows a nutrient profile in the modern oceans, where Zn is between ~0.04 and 0.5 nM in the surface layers, increasing

below the photic zone to ~8–10 nm, where it remains relatively constant down to the seafloor (Bruland *et al.*, 1994; Nolting & de Baar, 1994; Lohan *et al.*, 2002). Despite this variability, for the purposes of discussion we assume a concentration of 10 nM as a ‘modern’ value effectively describing the majority of the water column. While uptake in the photic zone could have led to surface-deplete nutrient-type Zn depth profiles in the deep past, especially if concentrations were limiting, the Zn concentration of deep waters obviously plays an important role in the upward diffusive resupply of Zn (John, 2007) and thus upper water column Zn concentrations.

In terms of the modern zinc budget, inputs from mid-ocean ridge hydrothermal systems ($\sim 4.4 \times 10^9$ mol year⁻¹) dominate riverine fluxes ($\sim 3.4 \times 10^8$ mol year⁻¹) by a factor of 13, while diffuse off-axis venting contributes little marine Zn ($\sim 1 \times 10^6$ mol year⁻¹) (Wheat *et al.*, 2002). However, the efficiency of scavenging of hydrothermal zinc is poorly constrained. Modern eolian Zn deposition is significant ($\sim 0.7\text{--}3.5 \times 10^9$ mol year⁻¹), although roughly 75% is anthropogenic (Duce *et al.*, 1991). Modern sinks are poorly constrained but likely include organic matter, metal hydroxides, and sulfide burial fluxes. Modern hydrothermal fluids, the primary natural Zn input, are enriched by 16 000–88 000 times the seawater Zn value at their source (Doe, 1994), but these values drop significantly with distance from the vent due to seawater dilution and Zn incorporation into sulfide and metal hydroxide phases (Trociene & Trefy, 1988; German *et al.*, 1991). Given higher mantle recycling rates (e.g., Sleep & Windley, 1982), we consider a hydrothermal Zn component to be more relevant during the Precambrian. Under anoxic and ferruginous (Fe-rich) seawater conditions, with Fe(II) > S(-II) as required for iron(III) oxyhydroxide formation, it is likely that hydrothermal Zn would have dispersed over wider areas of the deep ocean for a lack of an effective sink, with a spatial distribution and areal extent similar to Fe in the case of Precambrian iron formations (e.g., 10^6 km² in the Hamersley basin; Morris, 1993).

Based on the low solubility of Zn sulfide minerals and the formation of strong aqueous Zn–S complexes, expanded euxinia during the late Paleoproterozoic and Mesoproterozoic has been proposed to have limited the bioavailability of Zn and other sulfide-reactive trace metals (e.g., Cu, Cd) and thereby influenced metallome evolution (Sunda & Huntsman, 1995; Williams & da Silva, 1996; Saito *et al.*, 2003). However, recent work suggests that Proterozoic oceans were almost certainly laterally heterogeneous in their geochemical characteristics (e.g., Planavsky *et al.*, 2011), such that sulfidic conditions may have been limited to shallow or coastal areas (e.g. Poulton *et al.*, 2010). Such considerations therefore warrant a re-examination of trace metal evolution in the context of a dominantly ferruginous Proterozoic ocean, especially with regards to elements vital

for eukaryotic evolution such as Zn. Precambrian authigenic iron oxides, comprising laterally extensive IF that are highly Fe-rich and S-poor, necessitate Fe-rich and sulfide-poor conditions at the time of their deposition (Klein, 2005; Bekker *et al.*, 2010). In this regard, the Precambrian IF record may be considered to represent large areas with conditions where Fe(II) >> S(-II). Such chemical deposits thus record ancient seawater where no strong euxinic metal sink was locally present; this makes the IF record an ideal target for exploring paleomarine concentrations of Zn.

METHODS

Geochemical equilibrium calculations (Fig. 1) were performed using Visual MINTEQ 3.0 (Gustafsson, 2011), and the primary thermodynamic database provided (thermo.vdb) was modified to account for multiple aqueous Zn–sulfide complexes as well as Zn complexation by organic ligands (Table S1). Modeling conditions included seawater-like salinity (0.56 M NaCl), standard temperature (25 °C), the exclusion of molecular O₂ and a pCO₂ of ten times present atmospheric levels (PAL). Calcium, pH, and Fe were determined by equilibrium reactions with excess calcite and siderite. Redox considerations were omitted such that all Fe and S species are +II and -II, respectively. Supersaturated minerals were permitted to precipitate, and activity corrections were made using the Davies equation. Figure 1 presents chemical equilibrium models of speciation in the Fe(II)–S(-II)–Zn–organic–ligand system in terms of molar concentrations and mineral saturation indices (IAP/K_{sp}) and as a function of increasing total system sulfide concentration (sulfide in both dissolved form and bound in minerals). In this model, Fe(II) is available at concentrations in equilibrium with siderite (as per Holland, 1984), and pH is determined by equilibrium with siderite and calcite at pCO₂ = 10 × PAL (present atmospheric level). We consider a pCO₂ of ten times PAL as an intermediate value between high-end estimates for pre-1.8 Ga (>100 PAL, Ohmoto *et al.*, 2004) and the modern. Total zinc is fixed at an approximately modern value of 10⁻⁸ M (consistent with Zn concentrations derived from the IF record presented below, as well as those used by Saito *et al.*, 2003), and the system is effectively titrated with increasing quantities of sulfide (total S(-II) added).

Our data set of Zn in authigenic iron oxides includes new analyses and a comprehensive literature compilation (Table S2). We assign iron formations to one of four broad categories – Algoma IF, Superior IF, ironstones, and Phanerozoic hydrothermal deposits. Algoma IF are characterized by limited areal extent and close association with submarine volcanic sources. Superior IF are laterally extensive and typically formed on continental shelves. Ironstones encompass Precambrian granular and oolitic iron formations, as well as more modern iron oolite–pisolite

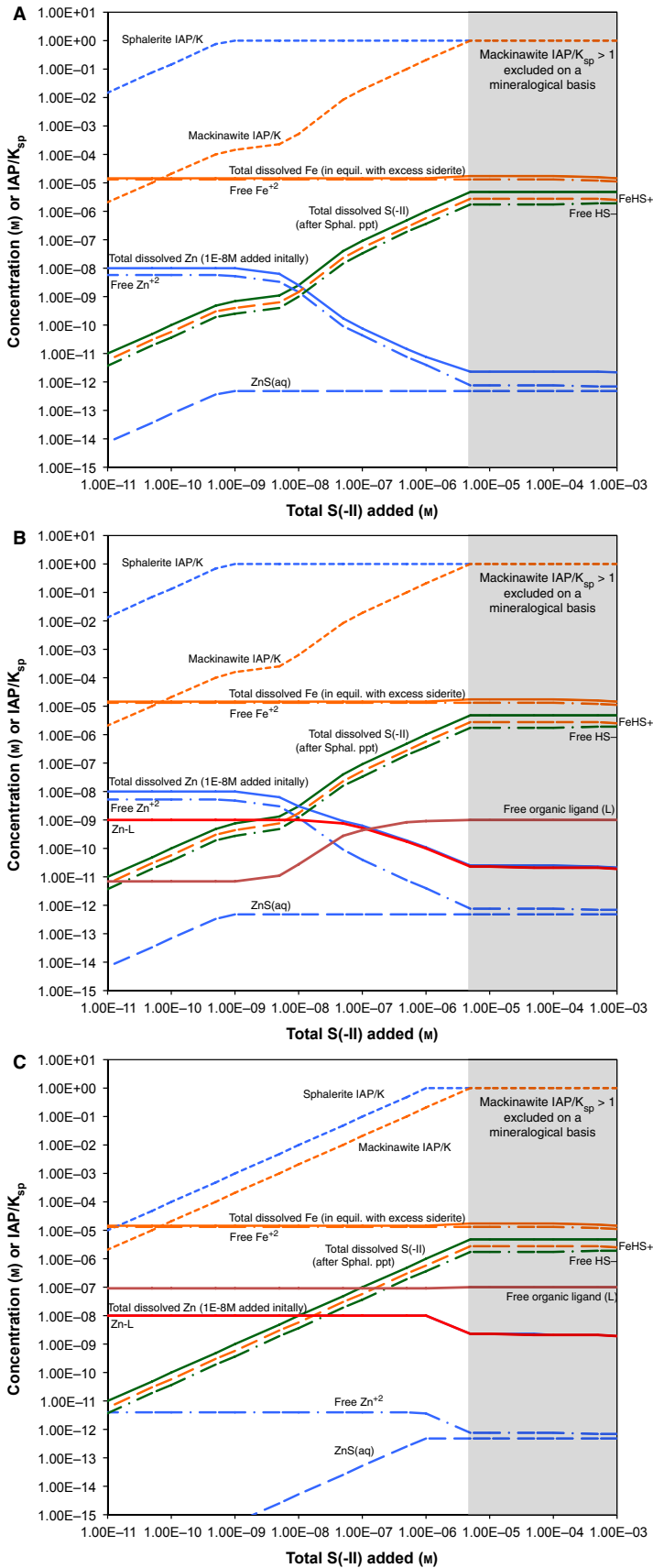


Fig. 1 Modeled chemical equilibrium concentrations for major Zn and Fe species and mineral saturation indices (IAP/ K_{sp}) as a function of total sulfide (HS^-) added for simulated seawater with (A) no organic complexation, (B) organic complexation as described for central north Pacific seawater (Bruland, 1989), and (C) same as (B) but with $100 \times$ higher organic ligand concentration. Blue lines represent inorganic Zn species, orange lines represent inorganic Fe species, green lines represent sulfide species, and red/burgundy lines represent organic ligands. Modeling was performed with visual MINTeq 3.0 (Gustafsson, 2011) under anoxic conditions, at $25^\circ C$, $0.56 M NaCl$ and a pCO_2 of ten times present atmospheric levels. Zn and Fe hydroxide and chloride species were also considered but are not plotted. The default thermodynamic database was adapted to account for multiple ZnS complexes and organic complexation (Table S1). Saturation with respect to calcite and siderite was assumed in all models and ultimately determined Ca and Fe concentrations, as well as pH, the latter ranging from 7.70 to 7.74 over the S(-II) range considered. Zn-S complexes included in Table S1, but not present in Fig. 1, are not indicated to exist at significant levels. Mineral saturation indices equal to one indicates saturation; in this model, supersaturation was not permitted, such that changes in total dissolved Zn and Fe are directly linked to mineral precipitation or dissolution. The gray area represents saturation with respect to Mackinawite and is excluded by the sulfide-deplete mineralogy of iron formations (IF).

occurrences that formed in shallow, nearshore environments. Phanerozoic hydrothermal deposits represent modern, oxic seawater deposits where Fe(III) deposition occurred near hydrothermal sources (Bekker *et al.*, 2010).

Zn was analyzed in drill core and fresh hand samples (i.e., samples collected in the field from outcrop), which were subsampled, then powdered and subjected to trace element analysis. Importantly, samples showing evidence of weathering, alteration or signs of severe metamorphic or diagenetic overprinting were excluded. Exclusion criteria include association with a lateritic profile, Fe concentrations greater than 60%, extensive veining, for all but Eoarchean samples recrystallization of chert to macrocrystalline quartz, intense folding, and above-greenschist facies metamorphism. Analyses were performed on powder digests or by *in situ* laser ablation (New Wave Research UP-213) using a Perkin Elmer Elan6000 Quadrupole – Inductively Coupled Plasma Mass Spectrometer (Q-ICP-MS) at the University of Alberta (U of A). Precision was monitored by repeated analyses of well-constrained international standards (BE-N Basalt, CRPG Nancy for digests and NIST SRM 610 or 612 for laser ablation). Sample analyses at Woods Hole Oceanographic Institute (WHOI) were conducted on a ThermoElectron Inc. Element 2 high-resolution sector field ICP-MS and precision and accuracy were assessed by the analysis of USGS geostandard BHVO-1. Sample selection and analytical methods are identical to our previous work (Konhauser *et al.*, 2009, 2011) and are described in detail therein. At the U of A, repeated analyses ($n = 3$) of BE-N produced a value for Zn of 128 ± 19 ppm at the two standard deviation level, compared with a recommended value of 120 ± 13 ppm.

Repeat analyses of laser ablation standards NIST SRM 610 and 612 at the U of A yielded average values of 474 ± 66 ppm ($n = 46$) and 38.7 ± 5.0 ppm ($n = 31$) at the single standard deviation level. These are compared with mean literature values for laser ablation of NIST STM 610 and 612 of 469 ± 34 ppm and 40 ± 2 ppm, respectively (Jochum *et al.*, 2011). At WHOI, repeated analysis of BHVO-1 produced a value for Zn of 91 ± 19 ppm at the two standard deviation level, compared with a recommended value of 105 ± 5 ppm.

From a database of over 3800 new and literature IF analyses, 1660 have available Zn data, and of those, 590 samples passed filters for detrital contamination ($<1\%$ Al_2O_3 and $<0.1\%$ TiO_2 ; Fig. 2) and compatible mineralogy; the unfiltered and filtered records are presented in Fig. 3A, B, respectively. Compatible mineralogies were restricted to Fe- and Si-rich chemical sediments, thereby excluding volcanics, sulfides, and carbonates. For authigenic iron oxide sediments with low detrital contamination, molar Zn and Fe data were compared with hypothetical partitioning scenarios to constrain potential paleomarine Zn concentrations.

The simple partitioning models presented herein (lines in Fig. 4) constitute an effort toward developing trace element proxies in IF that are better informed by the rock record itself and are independent of experimentally determined partition coefficients. The slope in Zn–Fe space (a Zn/Fe ratio) is calculated by assuming quantitative precipitation of both Zn and Fe from a given volume of seawater, such that hypothetical seawater Zn and Fe concentration scenarios may be compared directly with rock record data. In reality, only a fraction of total dissolved Zn will be removed at any given time, but as this is also the case with

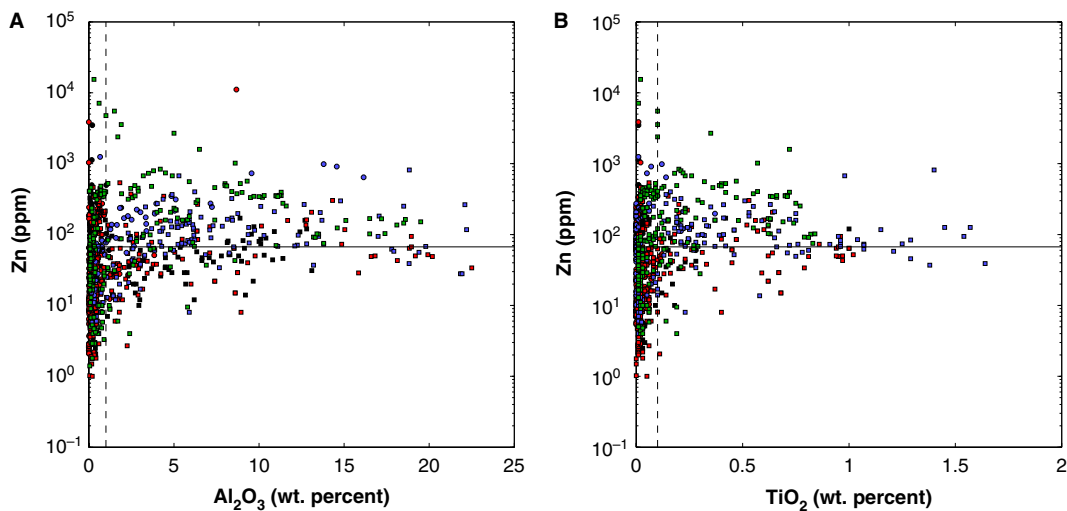


Fig. 2 Cross-plots of Zn vs. (A) Al_2O_3 and (B) TiO_2 . Dashed lines represent detrital contamination cutoffs of 1 and 0.1 weight percent for Al_2O_3 and TiO_2 , respectively. Black lines correspond to crustal values for Zn [67 ppm (Rudnick & Gao, 2003)] and indicate that above these cutoffs, Zn in iron formations (IF) approach crustal values. Colors correspond to varying IF types: Algoma (black), Superior (red), ironstone (blue), and Phanerozoic hydrothermal (green); c.f. methods. Additionally, circles represent laser ablation data, and squares indicate analyses after bulk digestion.

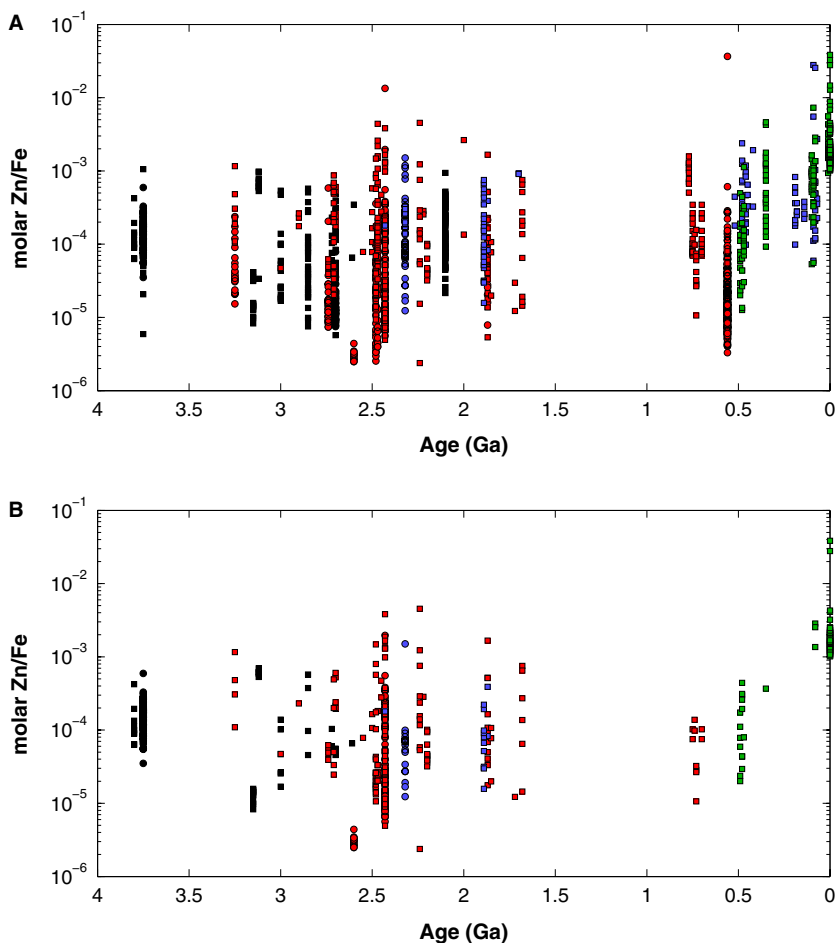


Fig. 3 (A) Unfiltered record of available molar Zn/Fe data in authigenic iron oxides through time, comprising Precambrian iron formation, Phanerozoic ironstones, and exhalites. When samples with appreciable detrital or hydrothermal influence are included in the record, there is a greater degree of variation than in the filtered record. (B) Molar Zn/Fe ratios in authigenic iron oxides, spanning Archean through Proterozoic iron formations (IF), Phanerozoic ironstones and exhalites; filtered for detrital contamination as per Fig. 2. Variability in Zn/Fe ratios at a given time may reflect heterogeneous marine Zn distributions, temporal variations (e.g., Zn drawdown during protracted deposition), or potential diagenetic modification. Importantly, no Zn/Fe data exist in our compilation that suggests the low, biolimiting dissolved Zn concentrations previously predicted by chemical equilibrium models for Precambrian oceans (Saito *et al.*, 2003). Symbols as per Fig. 2.

Fe, and as Zn adsorption depends on available Fe(III) oxyhydroxide surface sites, partial co-removal of Zn and Fe approaches the scenario of quantitative removal proposed by the simple, hypothetical partitioning scenarios.

The hypothetical partitioning scenarios presented in Fig. 4 are dependent on several important assumptions: (i) that adsorption occurred to Fe(III) oxyhydroxides, such that any particular trace element should scale with Fe (but not Si), (ii) that maximum dissolved Fe concentrations may be constrained (as per Holland, 1984) by either mineral solubility (e.g., $\sim 1\text{--}10$ ppm for siderite) or sedimentation rate (e.g., 20 mg cm^{-2} per year under a water column of at least 100 m, thus 2 ppm), and (iii) that Zn and Fe precipitated quantitatively. Assumption (i) is supported by Fig. 4, and while assumption (iii) is unlikely, it is conservative in that a maximum estimate of partitioning efficiency and thus a minimal potential seawater concentration is achieved.

RESULTS

Results of the geochemical models are presented in Fig. 1 and described in detail herein. Mineral saturation indices

(upper dashed lines) indicate that saturation with respect to sphalerite is achieved at total sulfide concentrations over 10^{-9} M and limits total dissolved Zn (combination of Zn^{2+} and ZnS) thereafter. Total sulfide concentrations above $5 \times 10^{-5}\text{ M}$ (saturation with respect to mackinawite) are effectively excluded by the S-poor mineralogy of IF samples. Three models are considered (i) in the absence of organic ligands (Fig. 1A), (ii) with 1 nM of an uncharacterized organic ligand-binding Zn^{2+} with a conditional log K of 11, as described for Central North Pacific seawater by Bruland (1989) (Fig. 1B), and (iii) with 100 nM of the same organic ligand, as a sensitivity test for historical differences in the availability of organic ligands (Fig. 1C). In all models, total Zn concentration is effectively limited by the sulfide-dependent solubility of sphalerite. In the absence of organic complexation (Fig. 1A), it can be seen that the hydrated metal aquo complexes of Zn^{2+} and Fe^{2+} dominate under all conditions, with the exception of the highest permitted sulfide concentrations, where Zn^{2+} and $\text{ZnS}_{(\text{aq})}$ become approximately equimolar (see Discussion). When organic complexation of zinc is considered, at modern concentrations of strong Zn-binding ligands ($\sim 1\text{--}3\text{ nM}$, Bruland, 1989; Jakuba *et al.*, 2012), organic zinc complexes

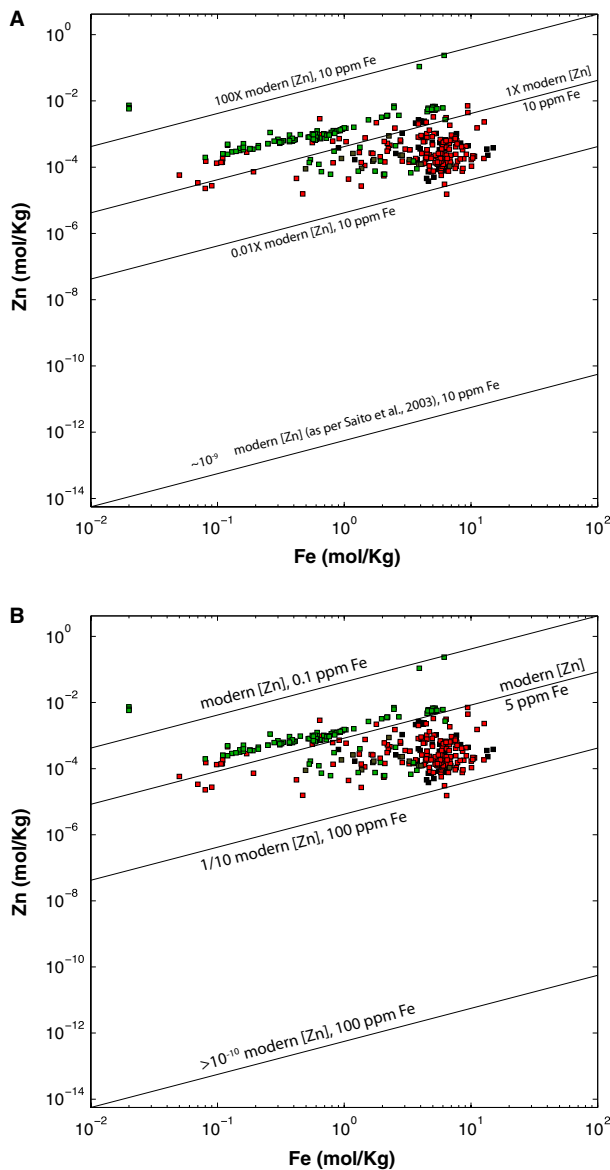


Fig. 4 (A) Zn–Fe cross-plot revealing paleomarine Zn partitioning recorded by the authigenic iron oxide record. Lines represent conservative models of Zn–Fe co-precipitation behavior for hypothetical paleomarine Zn and Fe reservoirs, including those previously predicted by chemical equilibrium modeling (Saito *et al.*, 2003). Near-modern paleomarine Zn concentrations are clearly indicated regardless of sample age. (B) Zn–Fe cross-plot further restricting paleomarine Zn concentrations under expanded boundaries of hypothesized paleomarine Fe conditions. Even at elevated Fe concentrations of $1790 \mu\text{M}$ (100 ppm), a dissolved Zn concentration of $\sim 1/10$ of modern (1 nM) is indicated. At low total Fe concentrations ($1.79 \mu\text{M}$), a dissolved Zn concentration of ~ 10 nM, effectively that of modern oceans, is still indicated. Symbols as per previous figures.

quickly become the dominant form of dissolved Zn. When total $S(-II)$ is further increased, sphalerite precipitation draws down the total dissolved reservoir to parity with the strong Zn-binding organic ligand (at $\sim 10^{-7}$ M total $S(-II)$ added). In the case of Zn-binding organic ligand concentrations

$100 \times$ that of modern (Fig. 1C), regardless of the ambient sulfide concentration, the total dissolved Zn pool is effectively dominated by organic complexes, free Zn^{2+} is suppressed even under sulfide-poor regimes, and the total Zn inventory is buffered against sphalerite precipitation losses. While these geochemical models reaffirm a strong role for organic complexation in determining the bioavailable Zn pool, bioavailable Zn^{2+} does not descend significantly below concentrations considered limiting for all organisms investigated (10^{-12} M), unless upper water column depletion of Zn is also considered (see Discussion).

Compositional data for modern and ancient authigenic iron oxides are presented in Figs 2–4. Zn concentrations in detritally filtered samples average 130 ppm (nearly twice the upper crustal value of 67 ppm; Rudnick & Gao, 2003), with average molar Zn/Fe ratios of 0.00228 and a standard deviation of 0.0238. For samples with Al or Ti values above detrital filter cutoffs, Zn concentrations tend toward upper crustal values, suggesting an increased Zn contribution from siliciclastic sources (Fig. 2); samples below detrital filter cutoffs lack correlation of Zn with Al and Ti but show Zn concentrations that scale with Fe (Fig. 4). This indicates authigenic Zn enrichment conforming to distribution coefficient behavior in these samples. It is likely that Zn was acquired during initial ferric oxyhydroxide precipitation by adsorption processes (e.g., Benjamin & Leckie, 1981), which, during the Archean and early Proterozoic, most likely occurred in the marine photic zone (Konhauser *et al.*, 2002; Kappler *et al.*, 2005; Planavsky *et al.*, 2010).

Figure 3A,B display all available data and those passing detrital filters, respectively, as a time series of molar Zn/Fe ratios. While significant variability exists at any given time, the overall trend is a relatively static range in Zn/Fe over geological time, except for the most modern samples (see Discussion). Figure 4A puts these ratios in perspective by presenting simple models for quantitative Zn removal at marine Fe concentrations of $179 \mu\text{M}$ (10 ppm) and near-modern Zn concentrations of 10 nM (0.65 ppb); nearly all data fall within the range predicted by our models and crucially indicate paleomarine Zn concentrations within an order of magnitude of modern oceans. An iron concentration of $179 \mu\text{M}$ was applied as it represents the upper limit of conservative estimates based on the work of Holland (1984) and would subsequently correspond to the lowest estimate of paleomarine Zn (i.e., decreasing Fe from 179 to $17.9 \mu\text{M}$ results in increasing estimates for paleomarine Zn).

At assumed Fe concentrations of $179 \mu\text{M}$, a minimum Zn concentration of 0.1 nM is indicated by Zn/Fe ratios preserved in ancient iron oxides, yet the majority of samples are well represented by a concentration within ten-fold of modern Zn values (Fig. 4A). Estimates are considered conservative as our models assume 100% adsorption of Zn onto the primary ferric oxyhydroxide; this quantitative

scavenging relationship represents maximum possible partitioning efficiency and thereby returns a minimum possible concentration; partial Zn adsorption would lead to increased estimates for paleomarine Zn concentrations. Conversely, increased dissolved Fe concentrations would result in a decreased estimate of paleomarine Zn concentrations. However, even at a high-end estimate of 1790 μM Fe, realistic only for essentially undiluted hydrothermal fluids (Edmond *et al.*, 1982) and $\sim 30 \times$ higher than limits imposed by siderite solubility (Holland, 1984), near-modern Zn levels are still indicated by the authigenic iron mineral record (Fig. 4B). There exists a high level of agreement between the filtered and unfiltered records in this regard (Fig. 3; Fig. S1).

DISCUSSION

Zn/Fe ratios in IF through time appear relatively constant (Fig. 3) despite dramatic changes in ocean chemistry from the Archean to today. The spread in Zn enrichments may be related to (i) vertical/lateral paleomarine spatial variability, (ii) local or short-term fluctuations in the marine Zn reservoir, or (iii) diagenetic effects. Firstly, it is anticipated that vertical/lateral spatial variability might be similar to that of modern oceans where Zn concentrations are heterogeneous between, and within, ocean basins. In terms of vertical distribution in the Precambrian, we expect that similar to today, enriched Zn fluids would resupply a depleted photic zone via diffusion and advection from deep waters. Future work examining Zn isotope compositions may reveal whether ancient upper water columns were depleted due to biological activity (c.f. Kunzmann *et al.*, 2013). As the precipitation of metastable IF precursor minerals (e.g., ferrihydrite) likely occurred in the photic zone (e.g. Konhauser *et al.*, 2002; Kappler *et al.*, 2005), it is possible that the spread in IF values record dynamics in depletion of the upper water column. Secondly, it is a possibility that variation within a single basin (and thus IF deposit) may be driven by potential pulse-like influxes of Zn along with Fe resulting from episodic hydrothermal activity as well as a potential drawdown of Zn due to protracted IF deposition. Events such as these may account for the highest and lowest Zn/Fe ratios, respectively. Thirdly, little information is available regarding further Zn adsorption or release upon iron mineral diagenesis or metamorphism. Experimental data indicate that for Zn–ferrihydrite co-precipitates, aging and mineral transformation, with or without added organics, has little effect on equilibrium Zn solubility (Martinez & McBride, 1999). With regards to metamorphism, Bhattacharya *et al.* (2007) presented a suite of IF data from the Jharkhand-Orissa region that showed similar Zn concentrations between hydrothermally metasomatized IF and ‘unaltered’ IF in the same region. In addition, samples used in our analyses were

devoid of obvious supergene alteration (i.e., severe chert re-crystallization, martite formation). These results, combined with the relatively coherent rock record data set provided here, suggest minimal post-depositional Zn mobilization in IF. Given the comprehensive nature of our data set, there are likely to be some samples that have been affected by secondary mineralization. Mineralization, however, is very unlikely to explain the overall trend of Zn abundances, a trend that differs from other elements that are commonly enriched during secondary mineralization (e.g., Cu, U) (Davidson & Large, 1994; Verma *et al.*, 2003; Tallarico *et al.*, 2005).

In addition to the three factors described above, variability in the IF record may reflect subtle changes in the reactivity of the solid-phase iron minerals for dissolved Zn. When considering only Precambrian data, linear regression between Zn and Fe is poorly supported (Fig. S1b); this may reflect variable contribution of less reactive and Zn-poor reduced iron minerals such as siderite or greenalite, which would also introduce variability in Zn/Fe ratios for any given deposit. Regression between Zn and Fe for Phanerozoic samples is more robust and along similar lines might reflect a fully oxidized and thus consistently zinc-reactive aspect of Phanerozoic hydrothermal iron precipitates. Indeed, a 10- to 100-fold increase in the Zn/Fe ratio of recent sediments may reflect the rapidity of Fe(III) precipitation under a fully oxygenated water column, resulting in increased contribution of Zn from enriched hydrothermal fluids proximal to modern vents. Under oxic conditions, iron mineral precipitation in closer proximity to hydrothermal sources, as well as a lack of co-precipitating reduced and thus Zn-poor iron mineral phases, could explain both the tighter relationship between Zn and Fe and the recent rise in Zn/Fe observed for the Phanerozoic.

In pyritic marine sediments, there is an apparent relationship between the degree to which a metal is preferentially hosted in pyrite (degree of trace metal pyritization, DTMP) and $\log K_{\text{metal-S}}/K_{\text{FeS}}$ (see Morse & Luther, 1999; their Fig. 3). This feature is akin to a linear free-energy relationship between the equilibrium partitioning of trace metals into pyrite and the equilibrium solubility of individual trace metal sulfide mineral phases and is characteristic of trace metal substitution into pyrite (Morse & Luther, 1999). Zn, as well as Cd and Pb, depart significantly from this trend in that they are anonymously low in concentration in the pyrite fraction of pyritic marine sediments, indicating that these elements are primarily sequestered as independent mineral phases rather than as a minor constituent of pyrite, likely as a natural consequence of the faster kinetics of their precipitation as metal sulfides (Morse & Luther, 1999). Accordingly, sphalerite (ZnS) solubility imposes an upper boundary on dissolved Zn in the presence of sulfide (e.g., Hsu-Kim *et al.*, 2008). The formation

of strong Zn–S complexes may further act to limit free Zn^{2+} under euxinic conditions (e.g., Landing & Lewis, 1992). Geochemical modeling (Fig. 1) demonstrates that under the ferruginous conditions necessary for the deposition of Precambrian IF, aqueous complexation and draw-down of bioavailable Zn^{2+} by sulfide may not be as important as previously thought. Saito *et al.* (2003) performed similar speciation calculations for Co, Fe, Mn, Zn, Ni, Cu, and Cd under hypothetical ‘ferro-sulfidic’ Archean ocean conditions and indicated that the vast majority (>99%) of dissolved Zn should be complexed with sulfide as $\text{ZnS}_{(\text{aq})}$. However, upon re-examination of Zn speciation for this study, it appears the conditional stability constant of the $\text{ZnS}_{(\text{aq})}$ species was not parameterized correctly in the study by Saito *et al.* (2003), leading to an overestimation of this species’ abundance, while the other metal species were correctly parameterized. In our current modeling effort, such high degrees of aqueous Zn complexation by sulfide do not occur until well after supersaturation with respect to mackinawite (FeS) is reached (Fig. 1). Such high sulfide concentrations are effectively excluded by the fact that, with the exception of some highly reduced Algoma-type iron formations, iron sulfide minerals are typically absent. A lack of correlation between Zn and S in our data set (see Fig. S2) further suggests a minimal role for S in Zn sequestration under Fe(III) oxyhydroxide depositional conditions. Several limitations also exist with respect to the thermodynamic modeling of Zn–S complexes. For instance, modeling is dependent on the stoichiometry of modeled Zn–S complexes and their respective stability constants; Rickard & Luther (2006) provide a short summary of Zn–S complexation and list eleven possible Zn–S complexes, several for which stability constants vary depending on the method used for determination.

In ancient oceans heterogeneous with respect to sulfide content (e.g., Poulton *et al.*, 2010; Planavsky *et al.*, 2011) and where sulfide effectively titrates iron such that the siderite-buffering effect inherent to our models no longer occurs, it is possible that bioavailable Zn would have been drawn down below biolimiting concentrations in sulfide-rich zones as per Saito *et al.* (2003). However, these zones were likely restricted to near-shore and other high productivity regions of the oceans (e.g., Poulton *et al.*, 2010). In such instances, Zn may have been buffered against sulfide by organic ligand complexation (Fig 1B,C), potentially becoming bioavailable again once reaching the overlying oxic or underlying ferruginous waters. It seems unlikely, given the consistency of the shales and IF record (Scott *et al.*, 2013; this work), that sulfide water masses controlled Zn bioavailability throughout much of the Precambrian. Accordingly, the Zn speciation model presented here for IF depositional conditions implies that bioavailable (non-complexed) Zn may well have been abundant and readily available to primitive eukaryotes.

An important alternative to the modeling described thus far is the possibility that strong and persistent organic complexes of zinc may have played an important role in controlling Zn solubility, speciation, and possibly bioavailability. This scenario is modeled in Fig. 1B,C and demonstrates that organic complexation of Zn plays a crucial role in determining the speciation of the reservoir, such that whenever the concentrations of strong Zn-binding organic ligands approach that of total dissolved Zn, organic Zn complexes will dominate the dissolved pool. Considering that poorly ventilated and reducing ocean conditions would have acted to stabilize strong organic ligands in seawater, such as those with reduced sulfur groups (e.g., thiols and cysteine-rich peptides), the possibility that organic complexation of Zn played a more important role in the Precambrian cannot be excluded. It therefore represents a strong caveat to the interpretations presented herein, potentially limiting the bioavailability of Zn. Interestingly in the modern ocean, strong Zn-complexing ligands appear only in the upper water column (Bruland, 1989; Jakuba *et al.*, 2012) where they are likely continually produced by microbial phytoplankton (Lohan *et al.*, 2002). By contrast, in the deeper oxygenated water column, these ligands are subsequently oxidized, and the sorbed Zn is released back into solution. How this potential scenario would have influenced the evolution of nutritional requirements is not clear; there are recent data indicating that the complexation of Zn by organic ligands can actually enhance phytoplankton Zn uptake (Aristilde *et al.*, 2012). Such high-affinity systems may have come at a metabolic cost, but could also have allowed access to this useful structural metal cation. It should be emphasized that the bioavailability of Zn–organic ligand complexes has a strong bearing on the interpretation of the second scenario. If Zn bound by organic ligands was indeed bioavailable in the Precambrian, it would suggest that under any of the conditions postulated here, Zn would be bioavailable to early eukaryotes. This would effectively represent a case where the two proposed scenarios become complementary.

The two chemical speciation scenarios presented here both constrain the bioavailable Zn inventory and have significant implications for paleomarine Zn geochemistry. In the first scenario where Zn speciation was not dominated by organic complexes, periods of ocean euxinia would have caused significant depletion of the oceanic Zn inventory due to precipitation of sphalerite with increased oceanic sulfide abundances (Fig. 1A). Such events may not have been captured by the IF record presented here due to the chemical incompatibility of extensive euxinia and the deposition of IF, but should be observable in parallel shale records (Scott *et al.*, 2013). Periods of expanded euxinia could have conceivably caused considerable oceanic Zn inventory instability, which itself could have been a temporal selection

pressure against early adoption of Zn ions in metalloenzymes. However, relatively stable sedimentary concentrations indicated by both the IF (this work) and shale records (Scott *et al.*, 2013) may be envisioned as a result of the second scenario, where oceanic Zn speciation is dominated by organic complexes such that the total Zn inventory would have remained stabilized despite large scale variations in the extent of euxinic marine conditions (Fig. 1C). Direct measurement of low-level Zn speciation conditions in analogous modern environments may contribute to our understanding of which of these scenarios may have dominated. Moreover, future modeling work is planned to better understand the factors controlling the aqueous complexation of zinc by sulfide and organic ligands, and their sensitivity to model presuppositions under ferruginous and euxinic ancient ocean chemistry scenarios.

The persistence of a zinc inventory on the order of magnitude of modern oceans throughout history is particularly curious given the late expansion of Zn-binding domains in eukaryotes (Dupont *et al.*, 2006, 2010). It is possible that the relatively late expansion of Zn-binding proteins over the course of eukaryotic metallome evolution reflected the regulatory needs inherent to increasingly complex genomes (see also Scott *et al.*, 2013). Late-evolving Zn-binding domains in eukaryotic genomes are predominately structural and localized to the nucleus, specifically in DNA-regulating elements (Dupont *et al.*, 2010). Power-law scaling of Zn-binding domains as a function of total proteome size is >1 for *Eukarya* but <1 for *Archaea* and *Bacteria* (c.f. Fig S1 from Dupont *et al.*, 2010). Essentially, eukaryotic genomes possess greater numbers of Zn-binding proteins with increasing genome size, while prokaryotic genomes follow the opposite trend, suggesting that the difference in metallome composition may reflect the dramatic differences in eukaryotic and prokaryotic genome regulation. The proliferation of structural, nucleus-bound Zn-binding domains should be expected to accompany rapid evolutionary innovation during late Proterozoic eukaryote diversification in body plans. Future phylogenetic work examining the expansion of eukaryotic Zn-binding domains in light of their specific roles in eukaryotic homeostasis may be able to confirm or deny such a hypothesis. Despite uncertainties relating to organic complexation of Zn in ancient oceans, this work provides important constraints and insight into the evolution of the Zn metallome, and the possibilities regarding intrinsic and biological influences, vs. extrinsic and geochemical, driving forces.

CONCLUSION

We conclude that the record of Zn enrichments in IF points toward a relatively constant marine Zn reservoir through geological time, with paleomarine concentrations within an order of a magnitude of modern values through-

out much of the Precambrian. Equilibrium speciation modeling reveals that under IF depositional conditions and modern organic ligand concentrations, the Zn reservoir should have been dominated by free and bioavailable Zn^{2+} , with aqueous Zn complexation by sulfide becoming important ($>50\%$ of the total dissolved reservoir) only at sulfide concentrations reaching FeS mineral saturation. Our finding of a near-modern bioavailable Zn reservoir through time as recorded by the IF record, and supported by detailed geochemical models, is also in line with that of the other common sedimentary proxy for paleomarine conditions, the euxinic shale record (Scott *et al.*, 2013). The agreement between these records testifies to the robustness of the model presented here. Furthermore, strong organic complexes of Zn, for example involving structures with reduced sulfur groups of high Zn affinity, may have been more important in ancient oceans for lack of an oxidative sink. This may have allowed stabilization of the Zn inventory through both ferruginous and euxinic ocean conditions, but potentially may have depressed Zn bioavailability, as the availability of Zn-organic complexation is not fully understood.

Together, this IF-based inventory and chemical speciation study places constraints on our understanding of the geochemical evolution of the Precambrian Zn reservoir and its potential coupling to eukaryotic metallome evolution. A novel possibility stemming from this work is that the late proliferation of Zn metalloenzymes in eukaryotes could have been a biologically intrinsic process related to the regulation of increasingly complex genomes, rather than solely dependent on the dramatic changes in the marine bioavailability of aqueous Zn species.

ACKNOWLEDGMENTS

We thank Guangcheng Chen for his assistance with laser ICP-MS and bulk digest analyses. We also thank the three anonymous reviewers for their insightful comments that have greatly improved this manuscript. This work was supported by a NSERC Discovery Grant to KOK, a NSERC PDF to SVL, a NSERC CGSM to LJR, and an NSF-EAR-PDF to NJP. MAS acknowledges support from the Gordon and Betty Moore Foundation Grant #2724. This work was also supported by grants from the Deutsche Forschungsgemeinschaft (DFG) to A.K. (KA 1736/4-1 and 12-1).

REFERENCES

- Anbar AD, Knoll AH (2002) Proterozoic ocean chemistry and evolution: a bioinorganic bridge? *Science* **297**, 1137–1142.
- Aristilde L, Xu Y, Morel FMM (2012) Weak organic ligands enhance zinc uptake in marine phytoplankton. *Environmental Science and Technology* **46**, 5438–5445.
- Bekker A, Slack JF, Planavsky N, Krapež B, Hofmann A, Konhauser KO, Rouxel OJ (2010) Iron Formation: the

- sedimentary product of a complex interplay among mantle, tectonic, oceanic and biospheric processes. *Economic Geology* **105**, 468–508.
- Benjamin MM, Leckie JO (1981) Multiple-site adsorption of Cd, Cu, Zn, and Pb on amorphous iron oxyhydroxide. *Journal of Colloid and Interface Science* **79**, 209–221.
- Berg JM, Shi Y (1996) The galvanization of biology: a growing appreciation for the roles of zinc. *Science* **271**, 1081–1085.
- Bhattacharya HN, Chakraborty I, Ghosh KK (2007) Geochemistry of some banded iron-formations of the archaean supracrustals, Jharkhand-Orissa region, India. *Journal of Earth System Science* **116**, 245–259.
- Brand LE, Sunda WG, Guillard RRL (1983) Limitation of marine phytoplankton reproductive rates by Zinc, Manganese, and Iron. *Limnology and Oceanography* **28**, 1182–1198.
- Bruland KW (1980) Oceanographic distributions of cadmium, zinc, nickel, and copper in the north pacific. *Earth and Planetary Science Letters* **47**, 176–198.
- Bruland KW (1989) Complexation of Zinc by natural organic ligands in the Central North Pacific. *Limnology and Oceanography* **34**, 269–285.
- Bruland KW, Orians KJ, Cowen JP (1994) Reactive trace metals in the stratified central North Pacific. *Geochimica et Cosmochimica Acta* **58**, 3171–3182.
- Coale KH, Michael Gordon R, Wang X (2005) The distribution and behavior of dissolved and particulate iron and zinc in the Ross Sea and Antarctic circumpolar current along 170°W. *Deep-Sea Research. Part I, Oceanographic Research Papers* **52**, 295–318.
- Crawford DW, Lipsen MS, Purdie DA, Lohan MC, Statham PJ, Whitney FA, Putland JN, Johnson WK, Sutherland N, Peterson TD, Harrison PJ, Wong CS (2003) Influence of zinc and iron enrichments on phytoplankton growth in the Northeastern Subarctic Pacific. *Limnology and Oceanography* **48**, 1583–1600.
- Davidson GJ, Large RR (1994) Gold metallogeny and the copper-gold association of the Australian Proterozoic. *Mineralium Deposita* **29**, 208–223.
- Doe BR (1994) Zinc, copper, and lead in mid-ocean ridge basalts, and the source rock control on Zn/Pb in ocean-ridge hydrothermal deposits. *Geochimica et Cosmochimica Acta* **58**, 2215–2223.
- Duce RA, Liss PS, Merrill JT, Atlas EL, Buat-Menard P, Hicks BB, Miller MJ, Prospero JM, Arimoto R, Church TM, Ellis W, Galloway JN, Hansen L, Jickells TD, Knap AH, Reinhardt KH, Schneider B, Soudine A, Tokos JJ, Tsunogai S, Wollast R, Zhou M (1991) The atmospheric input of trace species to the world ocean. *Global Biogeochemical Cycles* **5**, 193–259.
- Dupont CL, Yang S, Palenik B, Bourne PE (2006) Modern proteomes contain putative imprints of ancient shifts in trace metal geochemistry. *Proceedings of the National Academy of Sciences of the United States of America* **103**, 17822–17827.
- Dupont CL, Butcher A, Valas RE, Bourne PE, Caetano-Anollés G (2010) History of biological metal utilization inferred through phylogenetic analysis of protein structures. *Proceedings of the National Academy of Sciences* **107**, 10567–10572. doi: 10.1073/pnas.0912491107.
- Edgcomb VP, Molyneux SJ, Saito MA, Lloyd K, Böer S, Wilson CO, Atkins MS, Teske A (2004) Amelioration of metal toxicity by sulphide for Archaea at deep-sea hydrothermal vents. *Applied Environmental Microbiology* **70**, 2551–2555.
- Edmond JM, Von Damm KL, McDuff RE, Measures CI (1982) Chemistry of hot springs on the East Pacific Rise and their effluent dispersal. *Nature* **297**, 187–191.
- Franck VM, Bruland KW, Hutchins DA, Brzezinski MA (2003) Iron and zinc effects on silicic acid and nitrate uptake kinetics in three high-nutrient, low-chlorophyll (HNLC) regions. *Marine Ecology Progress Series* **252**, 15–33.
- Gardner LR (1974) Organic versus inorganic trace metal complexes in sulfidic marine waters – some speculative calculations based on available stability constants. *Geochimica et Cosmochimica Acta* **38**, 1297–1302.
- German CR, Campbell AC, Edmond JM (1991) Hydrothermal scavenging at the Mid-Atlantic Ridge: modification of trace element dissolved fluxes. *Earth and Planetary Science Letters* **107**, 101–114.
- Gustafsson JP (2011) Visual Minteq 3.0: <http://www2.lwr.kth.se/English/OurSoftware/vminteq>. (accessed on 10 October 2012).
- Holland HD (1984) *The Chemical Evolution of the Atmosphere and Oceans*. Princeton University Press, New Jersey.
- Hsu-Kim H, Mullaugh KM, Tsang JJ, Ucel M, Luther GW III (2008) Formation of Zn- and Fe-sulfides near hydrothermal vents at the Eastern Lau Spreading Center: implications for sulfide bioavailability to chemoautotrophs. *Geochemical Transactions* **9**, 6.
- Jakuba RW, Saito MA, Moffett JW, Bidigare B, Xu Y (2012) Dissolved zinc in the North Pacific: distribution, speciation, and importance to primary producers. *Global Biogeochemical Cycles* **26**, GB2015.
- Jochum KP, Weis U, Stoll B, Kuzmin D, Yang Q, Raczek I, Jacob DE, Stracke A, Birbaum K, Frick DA, Günther D, Enzweiler J (2011) Determination of reference values for NIST SRM 610–617 glasses following ISO guidelines. *Geostandards and Geoanalytical Research* **35**, 397–429.
- John SG (2007) The marine biogeochemistry of zinc isotopes. PhD thesis, MIT/WHOI, Cambridge, MA, 2007–2008.
- Kappler A, Pasquero C, Konhauser KO, Newman DK (2005) Deposition of banded iron formations by anoxygenic phototrophic Fe(II)-oxidizing bacteria. *Geology* **33**, 865–868.
- Klein C (2005) Some Precambrian banded iron-formations (BIFs) from around the world: their age, geological setting, mineralogy, metamorphism, geochemistry and origin. *American Mineralogist* **90**, 1473–1499.
- Konhauser KO, Hamade T, Raiswell R, Morris RC, Ferris FG, Southam G, Canfield DE (2002) Could bacteria have formed the Precambrian banded iron formation? *Geology* **30**, 1079–1082.
- Konhauser KO, Pecoits E, Lalonde SV, Papineau D, Nisbet EG, Barley ME, Arndt NT, Zahnle K, Kamber BS (2009) Oceanic nickel depletion and a methanogen famine before the Great Oxidation Event. *Nature* **458**, 750–753.
- Konhauser KO, Lalonde SV, Plaanavsky NJ, Pecoits E, Lyons TW, Mojzsis SJ, Rouxel OJ, Barley ME, Rosière C, Fralick PW, Kump LR, Bekker A (2011) Aerobic bacterial pyrite oxidation and acid rock drainage during the Great Oxidation Event. *Nature* **478**, 369–373.
- Kunzmann M, Halverson GP, Sossi PA, Raub TD, Payne JL, Kirby J (2013) Zn isotope evidence for immediate resumption of primary productivity after snowball Earth. *Geology* **41**, 27–30.
- Landing WM, Lewis BL (1992) Thermodynamic modeling of trace element speciation in the Black Sea. In: *Black Sea Oceanography* (eds Izdar E, Murray JW). NATO-ASI Series C, 351, Kluwer Academic Publishers, Netherlands, pp. 125–160.
- Landing WM, Burnett WC, Lyons WB, Orem WH (1991) Nutrient cycling and the biogeochemistry of manganese, iron and zinc in Jellyfish Lake, Palau. *Limnology and Oceanography* **36**, 515–525.
- Lohan MC, Statham PJ, Crawford DJ (2002) Total dissolved zinc in the upper water column of the subarctic North East Pacific.

- Deep-Sea Research. Part II, Topical Studies in Oceanography* **49**, 5793–5808.
- Luther GW, Rickard DT, Theberge S, Olroyd A (1996) Determination of metal (bi) sulfide stability constants of Mn^{2+} , Fe^{2+} , Co^{2+} , Ni^{2+} , Cu^{2+} , and Zn^{2+} by voltammetric methods. *Environmental Science & Technology* **30**, 671–679.
- Luther GW, Theberge SM, Rickard DT (1999) Evidence for aqueous clusters as intermediates during zinc sulfide formation. *Geochimica et Cosmochimica Acta* **63**, 3159–3169.
- Maret W (2001) Zinc biochemistry, physiology, and homeostasis—recent insights and current trends. *BioMetals* **14**, 187–190.
- Martinez CE, McBride MB (1999) Dissolved and labile concentrations of Cd, Cu, Pb, and Zn in aged ferrihydrite-organic matter systems. *Environmental Science and Technology* **33**, 745–750.
- Morris RC (1993) Genetic modeling for banded iron-formation of the Hamersley Group, Pilbara Craton, Western Australia. *Precambrian Research* **60**, 243–286.
- Morse JW, Luther GW III (1999) Chemical influences of trace metal-sulfide interactions in anoxic sediments. *Geochimica et Cosmochimica Acta* **63**, 3373–3378.
- Nolting RF, de Baar HJW (1994) Behaviour of nickel, copper, zinc and cadmium in the upper 300 m of a transect in the Southern Ocean (57°–62°S, 49°W). *Marine Chemistry* **45**, 225–242.
- Ohmoto H, Watanabe Y, Kumazawa K (2004) Evidence from massive siderite beds for a CO_2 -rich atmosphere before ~1.8 billion years ago. *Nature* **429**, 395–399.
- Planavsky NJ, Bekker A, Rouxel OJ, Kamber B, Hofmann A, Knudsen A, Lyons TW (2010) Rare Earth Element and yttrium compositions of Archean and Paleoproterozoic Fe formations revisited: new perspectives on the significance and mechanisms of deposition. *Geochimica et Cosmochimica Acta* **74**, 6387–6405.
- Planavsky NJ, McGoldrick P, Scott CT, Li C, Reinhard CT, Kelly AE, Chu X, Bekker A, Love GD, Lyons TW (2011) Widespread iron-rich conditions in the mid-Proterozoic ocean. *Nature* **477**, 448–451.
- Poulton SW, Fralick PW, Canfield DE (2010) Spatial variability in oceanic redox structure 1.8 billion years ago. *Nature Geoscience* **3**, 486–490. doi:10.1038/NNGEO0889.
- Rickard D, Luther GW III (2006) Metal sulfide complexes and clusters. *Reviews in Mineralogy & Geochemistry* **61**, 421–504.
- Rudnick RL, Gao S (2003) Composition of the continental crust. In: *Treatise on Geochemistry*, Volume 3 (eds Holland HD, Turekian KK). Elsevier Science, Amsterdam, Netherlands, pp. 1–64.
- Saito MA, Moffett JW, Chisholm SW, Waterbury JB (2002) Cobalt limitation and uptake in *Prochlorococcus*. *Limnology and Oceanography* **47**, 1629–1636.
- Saito MA, Sigman DM, Morel FMM (2003) The bioinorganic chemistry of the ancient ocean: the co-evolution of cyanobacterial metal requirements and biogeochemical cycles at the Archean-Proterozoic boundary? *Inorganica Chimica Acta* **356**, 308–318.
- Scott C, Planavsky NJ, Dupont CL, Kendall B, Gill B, Robbins LJ, Husband KF, Arnold GL, Wing B, Poulton SW, Bekker A, Anbar AD, Konhauser KO, Lyons TW (2013) Bioavailability of zinc in marine systems through time. *Nature Geoscience* **6**, 125–128.
- Shaked Y, Xu Y, Leblanc K, Morel FMM (2006) Zinc availability and alkaline phosphatase activity in *Emiliania huxleyi*: implications for Zn-P co-limitation in the ocean. *Limnology and Oceanography* **51**, 299–309.
- Sleep NH, Windley BF (1982) Archean plate tectonics: constraints and interferences. *The Journal of Geology* **90**, 363–379.
- Sunda W, Huntsman SA (1995) Cobalt and zinc interreplacement in marine phytoplankton: biological and geochemical implications. *Limnology and Oceanography* **40**, 1404–1417.
- Tallarico FHB, Figueiredo BR, Groves DI, Kositcin N, McNaughton NJ, Fletcher IR, Rego JL (2005) Geology and SHRIMP U-PB Geochronology of the Igarapé Bahia deposit, Carajás Copper-Gold Belt, Brazil: an Archean (2.57 Ga) example of Iron-Oxide Cu-Au-(U-REE) mineralization. *Economic Geology* **100**, 7–28.
- Tortell PD, Price NM (1996) Cadmium toxicity and zinc limitation in centric diatoms of the genus *Thalassiosira*. *Marine Ecology Progress Series* **138**, 245–254.
- Trocine RP, Trefy JH (1988) Distribution and chemistry of suspended particles from an active hydrothermal vent site on the Mid-Atlantic Ridge at 26°N. *Earth and Planetary Science Letters* **88**, 1–15.
- Verma MB, Roy MK, Saxena VP (2003) Uranium and polymetallic sulphide mineralisation in the banded iron formation at Udaisagar, Udaipur District, Rajasthan. *Journal of the Geological Society of India* **61**, 703–710.
- Wheat GC, Mottl MJ, Rudnick M (2002) Trace element and REE composition of a low-temperature ridge-flank hydrothermal spring. *Geochimica et Cosmochimica Acta* **66**, 3693–3705.
- Williams RJP, da Silva JJRF (1996) *The Natural Selection of the Chemical Elements*. Bath Press Ltd., Great Britain.
- Zirino A, Yamamoto S (1972) A pH-dependent model for the chemical speciation of copper, zinc, cadmium and lead in seawater. *Limnology and Oceanography* **17**, 661–671.

SUPPORTING INFORMATION

Additional Supporting Information may be found in the online version of this article:

Fig. S1. Molar Zn vs. Fe cross plots.

Fig. S2. Zn abundances plotted against molar Fe/S ratio.

Table S1. Equilibrium constants in the Zn-Fe-S-organic ligand system used for geochemical modeling in MINTEQ¹.

Table S2. Ti, Al, S, Zn, and Fe concentrations in ancient and modern authigenic iron oxides.